Silsesquioxane Molecules and Polystyrene Chains as a Model System for Colloid−Polymer Mixtures in the Protein Limit

Thomas Kramer, Ralf Schweins,† and Klaus Huber*

Universität Paderborn, Fakultät für Naturwissenschaften, Department Chemie, Warburger Str.100, D-33098 Paderborn, Germany

Received June 22, 2004; Revised Manuscript Received September 14, 2004

ABSTRACT: The present work investigates the structure of large polystyrene (PS) chains in two different solvents in the presence of octa-*n*-propylsilsesquioxane (SILS) molecules. Both solvents are good solvents for the PS chains. Viscosity measurements combined with static and dynamic light scattering revealed a significant shrinking of the PS chain dimensions, with increasing the SILS concentration. At the same time, chain−chain interactions decreased. Highly significant light scattering experiments became possible due to the fact that one of the solvents provided a refractivity which matched the scattering contrast of SILS, thus giving way to an unperturbed picture of the polymer chains. Together with the evaluation of the phase behavior of the PS−SILS mixture in toluene and in a θ-solvent, these results suggest that the PS−SILS mixture represents an interesting model system for colloid−polymer mixtures in the protein limit. Supplementing SANS experiments on SILS in solutions of perdeuterated toluene with perdeuterated PS chains clearly indicated a zone depleted of SILS. In line with this, the crystallization tendency of SILS was increased with increasing PS concentration due to a condensation of SILS in polymer-free domains.

Introduction

Along with the evolution of nanotechnology, mixtures composed of compact particles and polymeric chains in solution have attracted increasing interest among scientists. Denoted as colloid−polymer mixtures (CP), they turned out to be a widely spread phenomena, both in biological systems and in industrial products. Examples are stabilized pigment dispersions, the cytoskeleton, or the generation of exocellular polysaccharide chains by food-grade microorganisms in the presence of globular proteins during fermentation of dietary products.

Theoretical consideration of CP mixtures dated back to the pioneering work of Asakura and Oosawa.[1] They established the concept of depletion forces among colloids induced by the osmotic pressure of the polymeric chains. The osmotic pressure acts on zones between two neighboring colloids depleted from polymers because the respective intercolloidal distance dropped below the coil diameter. Meanwhile, a considerable body of theoretical and experimental work has been published on CP mixtures, summarized in valuable reviews.[2,3] A major part of this work dealt with the phase behavior of the colloids. Developments in the field took advantage of an interesting analogy between molecular systems on the one hand and the colloids dispersed in polymer solutions on the other hand. Noteworthy, a "gas−liquid" coexistence regime including a critical point was observed if the ratio R_g/R_c of the radius of gyration of the polymers R_g and the radius of the colloids R_c increased beyond 0.3. This underlines the importance of the R_g/R_c ratio as one of the characteristic variables determining the behavior of CP mixtures.

This size ratio R_g/R_c extends between two limiting cases: (i) In the so-called colloid limit, the spheres are much larger than the polymer chains. In fact, the original model and a large fraction of the work devoted to CP mixtures deals with this limit. (ii) In the protein limit, the colloids are much smaller than the chains. The name derives from the occurrence in various biological systems, where small globular proteins adopting the role of the colloids exist in the presence of larger coils. As expected, theories on CP mixtures, which are developed for $R_c > R_g$, fail in the protein limit. It was de Gennes,[4] who, by means of scaling arguments, first pointed out that it is much harder to invoke phase separation in the case of the protein limit. Yet, first experiments on biological systems[5] indicate immiscibility also for systems with $R_g/R_c \gg 1$. Recent theoretical progress and computer simulations confirmed these observations. It could be demonstrated that immiscibility curves in a volume fraction diagram are shifted to higher values of colloid volume fractions if the solvent quality is getting better.[6−8] For low colloid contents these curves extend into the regime of semidilute solution of the polymer chains. Like in the case of $R_g < R_c$, the main focus of research on CP mixtures in the protein limit lay on the colloid component. On length scales larger than the colloids, the solvent can be considered to be effectively structureless and addition of small colloids simply decreases the solvent quality. As a consequence of this worsening of the solvent quality, an interesting feature of the polymer chains is predicted.[9,10] Excluded-volume effects between the polymer segments and the colloidal particles may cause the single chains to shrink or collapse if immiscibility occurs.

Only one work is known to the authors, which explicitly considers the structure of the polymer chains in CP mixtures,[11] and no experimental work exists on a coil collapse induced by an increasing amount of small colloidal particles. Part of the reason for this deficiency is the lack of convenient model systems, which permit an experimental access of the polymer structure in the protein limit. The development of an appropriate model

† Institut Laue-Langevin, LSS Group, B.P. 156, 6, rue Jules Horowitz, F-38042, Grenoble, Cedex 9, France.

* To whom correspondence should be addressed. E-mail huber@chemie.uni-paderborn.de; Ph +49-5251-602125; Fax +49-5251-604208.

10.1021/ma048766x CCC: $30.25
Published on Web 12/09/2004

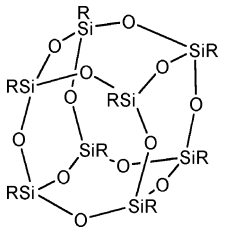

Figure 1. Chemical structure of a SILS molecule. The eight silicium atoms are placed in the corners of a cube; the lateral oxygen edges are pulled outward due to the bond angles differing from 90° and 180°. For R = *n*-propyl, Veprek et al.[20] calculated the diameter of this molecule to 1.41 nm.

system does not only depend on the selection of monodisperse colloids small enough compared to the size of the polymer chains. In addition, the colloids must not disturb an independent characterization of the coexisting polymer chains.

If characterization of the polymer chains is performed by light scattering, the colloidal spheres should preferably approach isorefractivity with the solvent. As important as isorefractivity of the colloids is the availability of small colloids having radii of 20 nm and smaller. Different methods have been established to achieve this synthetic goal, but not all procedures led to nanoparticles being suitable for the present investigation. For instance, nanoparticles made of inorganics, e.g. $CaCO_3$ or AgCl, have refractive indices[12,13] which are too large to still be matched with common organic solvents. Organic colloids with a lower index of refraction are for example based on acrylate or styrene monomers.[14] Another system with an inherent capability to become isorefractive is based on silicate. The synthesis of small polyorganosiloxane microgels is achieved by hydrolyzation and condensation of multifunctional silanes in the presence of a catalyst and a special surfactant, namely benzethonium chloride.[15−17]

The present work pursues two goals: (i) the selection of an appropriate CP model system representing the protein limit and (ii) an investigation of the polymer component at variable colloid concentration by means of light and neutron scattering and viscosimetry.

Octa-*n*-propylsilsesquioxane molecules abbreviated as SILS (Figure 1) are used as model spheres to investigate the protein limit. The samples consist of large polystyrene (PS) chains and SILS, where the size ratio varies between $25 < R_g/R_c < 110$. Several aspects make this system a preferable choice to investigate the protein limit of colloid polymer mixtures: (1) Chemical relationship between SILS and silica based colloids may help to find an isorefractive solvent.[11] (2) The SILS molecule is highly symmetrical and represents a small sphere to a good approximation. (3) Mass and size distributions of SILS are monodisperse, contrary to most other small colloidal systems. (4) SILS molecules have a diameter close to the Kuhn length of PS. The respective ratio of sphere diameter to Kuhn length is comparable to the one used in theoretical considerations dealing with the protein limit, where a collapse of the polymer chain is proposed.[10] (5) The relatively simple synthesis of the molecules makes accessible large amounts of this compound.

Two different solvents are used to investigate the PS chains in solution in the presence of SILS: (i) pure toluene and (ii) a mixture of toluene (50 vol %) and ethyl acetate (50 vol %) (Tol−EthAc). The two solvents are chosen in order to generate different scattering contrasts for the dissolved SILS molecules. It is known that polyorganosiloxane microgels become isorefractive in the Tol−EthAc mixture,[11] whereas an additional scattering contrast has to be considered in toluene.[18] The chemical similarity between SILS and polyorganosiloxane molecules justifies the expectation that the scattering behaviors of SILS and polyorganosiloxane microgels are comparable.

Following a detailed Experimental Section, the paper first outlines the characteristics of pure SILS solutions, where the SILS molecules are compared to ideal hard spheres. On the basis of these results, the SILS polymer chain mixtures are investigated by discussing Staudinger indices, solvent qualities, and chain dimensions. Structural investigations are dominated by light scattering at varying contrast conditions and supplemented by small-angle neutron scattering (SANS) experiments on SILS dissolved in fully matched solutions of D8-PS in D8-toluene. The work is completed by a preliminary investigation of the crystallization behavior of SILS in the presence of PS and the phase behavior of SILS/PS under variable solvent conditions. Results reveal characteristic features of a protein limit.

Experimental Details and Data Evaluation

Preparation of Octa-*n*-propylsilsesquioxane (SILS). Octa-*n*-propylsilsesquioxane is prepared according to a standard procedure described in several publications.[19−21] *n*-Propyltrichlorosilane (ABCR, Karlsruhe, Germany) is added dropwise to methanol (technical grade) and hydrolyzed by slowly adding concentrated hydrochloric acid (Merck, Darmstadt, Germany) into the solution. After 20 days the obtained crystals are washed several times with methanol and dissolved in benzene to allow freeze-drying. The obtained SILS is characterized by ^{1}H, ^{13}C, and ^{29}Si NMR in C_6D_6 as the solvent.[21]

Linear Polymer Chains. Linear hydrogenated and deuterated polystyrene (PS) chains are purchased from Polymer Standards Service (Mainz, Germany) and Macherey-Nagel (Düren, Germany). Details are summarized in Table 3. The behavior of PS chains in solution is investigated in the presence of different amounts of SILS by means of viscosimetry, light scattering, and small-angle neutron scattering. In the latter case, fully deuterated PS samples are used.

Solvent Systems for PS Chain Characterization. Two solvent systems are chosen to investigate PS chains in the presence of SILS: pure toluene and a mixture of toluene (50 vol %) and ethyl acetate (50 vol %), from now on referred to as Tol−EthAc. Toluene and ethyl acetate (both from Merck) are distilled prior to use. Because of the chemical relationship of SILS with polyorganosiloxanes, the system SILS in Tol−EthAc is expected to be closer to isorefractivity than SILS in toluene.[11,18]

Refractive Index Measurements. Measurements are performed at room temperature with a scanning interferometric refractometer (Nanofilm Technology, Göttingen, Germany) operating at a wavelength of 543.5 nm. The measuring cell has a volume of 6.2 μL. Usually, the index of refraction n is measured for six or more concentrations c. The slope of a plot n vs c leads to the respective refractive index increment.

Density Measurements. To calculate dynamic viscosities according to eq 2, densities of pure solvents and of SILS solutions are required. They are determined with a vibrating tube densitometer (Paar Digitale Präzisionsdichte-Messeinrichtung, DMA 02 D). The temperature is controlled by a thermostat (Lauda, Germany) with a precision of ±0.1 K. The resonance frequency of the tube is specified by the mass of the tube plus the mass of the fluid inside. For each sample the resonance frequency is measured 10 times. The densitometer is calibrated with water and air as fluid systems with known densities.

Table 1. Density and Viscosity of SILS Solutions in Toluene and Tol−EthAc at Different Temperatures[a]

parameter	solvent: toluene	solvent: Tol−EthAc
temperature [°C]	25	25
density ρ [kg/m^3]	$861.75 + 0.244c$	$878.63 + 0.202c$
viscosity η [Pa s]	$5.657 \times 10^{-4} + 7.757 \times 10^{-7}c + 3.723 \times 10^{-9}c^2$	$4.717 \times 10^{-4} + 1.253 \times 10^{-6}c$
fitted regime [g/L]	$0 < c < 350$	$0 < c < 200$
temperature [°C]	40	
density ρ [kg/m^3]	$846.61 + 0.226c$	
viscosity η [Pa s]	$4.737 \times 10^{-4} + 6.876 \times 10^{-7}c + 2.178 \times 10^{-9}c^2$	
fitted regime [g/L]	$0 < c < 300$	

[a] c_{SILS} (c) is given in g/L. Corresponding viscosity measurements are shown in Figure 2.

Density measurements of SILS solutions are carried out in toluene and Tol−EthAc. In both cases a linear dependence of the density on SILS concentration can be observed. Table 1 gives the parameters a and b of the linear equation

$$\rho = ac_{SILS} + b \tag{1}$$

with ρ being the density and c_{SILS} the SILS concentration in g/L.

Viscosity Measurements. Dynamic viscosities are measured using a typical Ostwald capillary viscometer (Schott Geräte, Hofheim a.Ts., Germany). The capillary is thermally adjusted in a water bath by a thermostat (Lauda, Germany) with a precision of ±0.1 K. For each concentration the time needed for a predefined volume to flow through the capillary is measured five times. After application of Hagenbach's correction, the corrected averaged flow times $\bar{t}$ are directly related[22] to the dynamic viscosity η.

$$\eta = K\rho\bar{t} \tag{2}$$

In eq 2, K is a viscometer constant, determined by calibrating the viscometer with five fluids, and ρ is the density of the investigated solutions determined according to eq 1. It should be mentioned that K and ρ are temperature-dependent.

In the present work, dynamic viscosities of SILS solutions and of PS chains in SILS free solutions and in SILS solutions are measured for the following reasons: (i) transformation of diffusion coefficients of PS chains from dynamic light scattering into hydrodynamically effective radii R_h requires the respective viscosity of the SILS solution; (ii) information about the shape of SILS in solution can be obtained from viscosities of concentration series of SILS solutions; (iii) beside light scattering, viscosimetry is used as a second method to investigate the behavior of PS chains in the presence of different SILS concentrations.

Therefore, dilution series of PS chains consisting of at least five PS concentrations and the respective SILS solution acting as the solvent are measured. Extrapolating reduced viscosities $|\eta|$

$$|\eta| \equiv \frac{\eta_{solution} - \eta_{solvent}}{c_{PS}\eta_{solvent}} \tag{3}$$

to zero PS concentration leads to the Staudinger index $[\eta]$ of the PS coils.

$$|\eta| = [\eta] + mc_{PS} \tag{4}$$

Table 2 summarizes the slopes m and Staudinger indices $[\eta]$ of all measurements.

Light Scattering Experiments. All scattering experiments are performed with a model 5000e compact goniometer system from ALV-Laser Vertriebsgesellschaft (Langen, Germany), which permits the simultaneous recording of static and dynamic light scattering. A Nd:YAG laser with 100 mW operating at a wavelength of 532 nm is used as a light source.

Table 2. Parameters of a Linear Fit (Eq 4) from the Dependence of the Reduced Viscosity on PS Concentration c [g/L] of Sample PS-2.5M at 25 °C (Figure 3)[a]

c_{SILS} [g/L]	slope m [L^2/g^2]	$[\eta]$ [L/g]
	Toluene	
0	0.081	0.503
52	0.075	0.461
100	0.073	0.455
152	0.057	0.391
196	0.050	0.358
249	0.047	0.307
305	0.032	0.270
352	0.029	0.212
	Tol−EthAc	
0	0.074	0.414
69	0.059	0.384
147	0.051	0.337
192	0.050	0.293

[a] Measurements are performed in two solvents with varying amounts of silsesquioxane c_{SILS}.

Cylindrical quartz glass cuvettes with an outer diameter of 20 mm serve as scattering cells. The scattering intensity is observed in an angular range of 30°−150°. The temperature of the cell housing is controlled by a thermostat (Haake, Germany) with a precision of ±0.01 K. All samples are filtered through PTFE syringe filters (Macherey-Nagel, Düren, Germany). For solutions containing PS chains with M_w > 1 000 000 g/mol a pore size of 0.45 μm is applied. In the case of all other solutions and solvents, filters with a pore size of 0.2 μm are used.

Light scattering experiments are carried out to investigate the conformation of PS chains in toluene and Tol−EthAc at different concentrations of SILS. At each SILS concentration five PS concentrations are measured to allow extrapolation to infinite dilution. If represented according to Zimm's approximation,[23a] the static light scattering (SLS) data read

$$\frac{Kc}{\Delta R_\theta} = \frac{1}{M_w P(q)} + 2A_2c \tag{5}$$

with M_w the weight-averaged molecular weight, $P(q)$ the form factor, A_2 the second osmotic virial coefficient, and c the polymer concentration in g/L. The scattering intensity of the samples is expressed in terms of the Rayleigh ratio ΔR_θ. The contrast factor K is defined as

$$K = \frac{4\pi^2}{\lambda_0^4 N_A}\left(n\frac{dn}{dc}\right)^2 \tag{6}$$

In eq 6, λ_0, N_A, n, and dn/dc are the laser wavelength in vacuum, Avogadro's number, the refractive index of the solvent, and the refractive index increment of the polymer, respectively. The scattering vector q is defined as

$$q = \frac{4\pi n}{\lambda_0}\sin\frac{\theta}{2} \tag{7}$$

with θ the scattering angle. For particles significantly smaller than the wavelength, $1/P(q)$ can be approximated by

$$\frac{1}{P(q)} \cong 1 + \frac{R_g^2}{3}q^2 \tag{8}$$

with R_g^2 being the z-averaged mean-square radius of gyration.

In the case of polymer chains under good solvent conditions, data from SLS experiments are preferably evaluated according to Berry's[23b] approximation

$$\sqrt{\frac{Kc}{\Delta R\theta}} = \sqrt{\frac{1}{M_w}}\left[1 + A_2M_wc + \frac{R_g^2q^2}{6}\right] \tag{9}$$

Table 3. Characteristics of Linear PS Chains Used in Mixing Experiments[a]

PS sample	supplier	solvent	T [°C]	$M_w \times 10^{-3}$ [g/mol]	R_g [nm]	R_h [nm]	$A_2 \times 10^7$ [mol L g^{-2}]
PS-2.5M	PSS	toluene	25	2400	78	55	1.636
		toluene	40	2700	76	56	2.265
		Tol/EthAc	25	2030	72	47	1.513
PS-900K	M+N	toluene	25	870	40	27	3.044
		Tol/EthAc	25	740	37	23	2.674
PS-250K	PSS	toluene	25	270	17	14	4.061
		Tol/EthAc	25	240	16	11	3.191
D8-PS	PSS	toluene	25	1066	58	38	2.886

[a] M_w, R_g, A_2 and R_h are gained from light scattering experiments. All values are obtained by extrapolating to zero PS concentration. Abbreviations: PSS (Polymer Standards Service); M+N (Macherey-Nagel).

Table 4. Solvent Properties Used in Viscosimetry and Light Scattering

solvent	T [°C]	ρ [g/mL]	η [mPa s]	n[32,33]	$(dn/dc)_{PS}$ [mL/g]
toluene	25	0.862	0.5565	1.496	0.110[30]
toluene	40	0.849	0.4755	1.496	0.117[30]
Tol−EthAc	25	0.876	0.4860	1.431	0.164

Extrapolated values of R_g, M_w, and A_2 for all investigated PS samples are summarized in Table 3. To guarantee dilute solution behavior of the PS chains, their concentration regime is kept below the so-called overlap concentration calculated according to eq 10

$$c^* = \frac{M_w}{\frac{4}{3}\pi R_g{}^3 N_A} \tag{10}$$

Dynamic light scattering (DLS) reveals the z-averaged diffusion coefficient D. To this end, the electric field time correlation functions are evaluated by the cumulant analysis derived by Koppel.[24] The diffusion coefficients are transformed into hydrodynamically effective radii R_h via the Stokes−Einstein equation

$$R_h = \frac{kT}{6\pi\eta}\frac{1}{D} \tag{11}$$

with k being Boltzmann's constant, T the temperature, and η the solvent viscosity. Since SILS solutions are used as solvents for the polymer chains, the viscosities of different SILS concentrations have to be determined. Table 1 gives the relationship between viscosity and SILS concentration as linear (Tol−EthAc) or quadratic (toluene) fits.

The CONTIN analysis developed by Provencher yields information about the distribution of relaxation times.[25] It is used to inspect the size distribution of the respective samples.

Small-Angle Neutron Scattering. Measurements are performed at the high flux reactor of the Institut Laue-Langevin (ILL) in Grenoble, France. The experiment is done at the small-angle neutron scattering instrument D11. Scattering intensities are recorded with a two-dimensional position-sensitive ^{3}He detector, which consists of a matrix assembly of 64 × 64 cells of 1 cm^2. Four different instrument settings are used in order to cover a broad q range: a neutron wavelength of 4.51 Å with a sample−detector distance of 1.1 m and a neutron wavelength of 6 Å with sample−detector distances of 2.5, 10, and 34 m. These four settings correspond to a scattering vector regime of 1.8×10^{-3} Å$^{-1} < q < 0.45$ Å^{-1}.

All samples are measured at 25 °C. The calibration standard (H_2O) is put in a Hellma cell of 1 mm path length, whereas the solvents as well as the solutions are put in cells with 2 mm path length.

The transmission of the samples is determined by measuring the direct, attenuated beam (scattering vector $q = 0$) passing through any object (I_x), divided by the analogous measurement of the incident beam (I_i):

$$T_x = \frac{I_x(q=0)}{I_i(q=0)} \tag{12}$$

After determination of the central detector coordinates for each sample−detector distance, the two-dimensional raw data are radially averaged. Averaged data are normalized by use of the known wavelength-dependent effective differential cross section of H_2O (tabulated for D11 ^{3}He detector:[26] $d\Sigma/d\Omega_{H_2O} = 0.905$ cm^{-1} for $\lambda = 6$ Å and 0.857 cm^{-1} for $\lambda = 4.51$ Å).

The differential scattering cross section per unit volume of the solutions and the solvent are separately calculated according to the following equation:[27]

$$\left(\frac{d\Sigma}{d\Omega}\right)_S = \frac{(I_S - I_{Cd}) - \frac{T_{S+EC}(1-n_S\tau)}{T_{EC}(1-n_{EC}\tau)}(I_{EC} - I_{Cd})}{(I_{H_2O} - I_{Cd}) - \frac{T_{H_2O+EC}(1-n_{H_2O}\tau)}{T_{EC}(1-n_{EC}\tau)}(I_{EC} - I_{Cd})} \frac{T_{H_2O+EC}(1-n_{H_2O}\tau)\cdot 0.1\cdot\left(\frac{d\Sigma}{d\Omega}\right)_{H_2O}}{T_{EC}(1-n_{EC}\tau)\cdot 0.2} \tag{13}$$

The indices denote sample (S), corresponding to solvents or solutions, standard (H_2O), empty cell (EC), and cadmium (Cd). The cadmium measurement provides the electronic background. The term $(1 - n\tau)$ takes into account the correction for dead time losses with n being the integral count rate of each measurement and τ being the dead time.

The system under investigation consists of fully deuterated PS (see Table 3 for details) dissolved in deuterated toluene (Deutero, Kastellaun, Germany) at constant SILS concentration. The D8-toluene/SILS mixture serves as the solvent for D8-PS. A dilution series of four PS concentrations and the solvent have been measured with the above-stated configuration. To allow extrapolation to infinite dilution, the net intensities of the D8-PS samples have to be calculated by using

$$\Delta\left(\frac{d\Sigma}{d\Omega}\right)_{sample} = \left(\frac{d\Sigma}{d\Omega}\right)_{solution} - \left(\frac{d\Sigma}{d\Omega}\right)_{solvent} \tag{14}$$

Further consideration of the incoherent scattering is obsolete, since D8-PS and D8-toluene are fully matched and no extra incoherent scattering stemming from the D8-PS is observable. By applying eq 14, absolute net intensities are gained.

Crystallization and Phase Behavior. The crystallization behavior is investigated by dissolving solid PS in a solution of SILS in toluene. Starting from a transparent solution at high temperature, the temperature is decreased stepwise until turbidity occurs. Crystals are formed after allowing the samples to equilibrate at this temperature. The phase diagrams of PS in SILS/(toluene or cyclohexane) are obtained in a similar way. The solutions are kept at 50 °C for 3 h and subsequently cooled in a tempered water bath to 25 °C (toluene) or to the θ temperature of PS 35 °C (cyclohexane). The resulting precipitates do not show solidlike crystals, except for very low PS concentrations at high c_{SILS} in toluene.

Results and Discussion

SILS Solutions. According to Einstein,[28] the viscosity of a solution of an ideal hard sphere only depends on the volume fraction Φ occupied by the spheres irrespective of their size. He found

$$\eta_{\text{solution}} = \eta_{\text{solvent}}(1 + 2.5\Phi) \tag{15}$$

where Φ is the volume fraction calculated as follows

$$\Phi = \frac{4\pi R^3 c N_A}{3M} \tag{16}$$

with c being the concentration in g/L, and M and R the molar mass and the radius of the respective sphere. The factor $4\pi R^3/3$ is the hydrodynamically effective volume of the dissolved particles, which in the case of ideal spheres corresponds to the sphere volume. The latter can be estimated according to the following procedure.

According to eq 4, the viscosity measurements of SILS solutions in toluene and Tol−EthAc can be described as

$$|\eta| = [\eta] + mc_{\text{SILS}} \tag{17}$$

SILS is readily soluble in both pure toluene (up to 400 g/L) and Tol−EthAc (up to 200 g/L), permitting high volume fractions to be investigated. The solubility can even be enhanced by increasing the temperature. If the SILS molecules behave like ideal hard spheres, their reduced viscosity should be independent of the SILS concentration. As can be seen in Figure 2, the dependence on SILS concentration is only marginal, with slopes $m < 5.2 \times 10^{-6}$ L^2/g^2 for all three cases. Inserting eq 16 into eq 15 and eq 15 into eq 3 leads to

$$\frac{4\pi R^3}{3} = [\eta]\frac{M}{2.5} \tag{18}$$

which enables to calculate the radius of the SILS molecule by using the Staudinger index in the limit of $c_{\text{SILS}} = 0$ g/L. In both solvent systems, eq 18 yields a radius of 0.6 nm for the SILS molecule. Veprek et al.[20] calculated the radius of octa-*n*-propylsilsesquioxane to 0.705 nm, being in good agreement with the estimation according to eq 18.

Behavior of PS Chains in SILS Solutions. Three methods have been applied to investigate PS chains: viscosimetry, light scattering, and SANS. In all cases, dilution series of PS chains have been examined in order to enable extrapolation to infinite dilution.

Figure 3 shows the dependence of the reduced viscosity $|\eta|$ (eq 3) on the PS concentration c_{PS} for sample PS-2.5M at various predefined SILS concentrations c_{SILS} in both toluene and Tol−EthAc. In the case of SILS free solutions, the reduced viscosity increases slightly with decreasing c_{PS} below $c_{\text{PS}} = 0.5$ g/L. This behavior has already been observed in 1961 and has been ascribed to the method and not to single chain behavior.[29] Thus, the concentration regime $c_{\text{PS}} < 0.5$ g/L has been ignored for the extrapolation of $|\eta|$ toward $c_{\text{PS}} = 0$.

Results in pure toluene can be used to estimate the molecular weight of the PS sample. Applying the Mark−Houwink equation

$$[\eta] = KM^a \tag{19}$$

with $K = 7.5 \times 10^{-6}$ L/g and $a = 0.75$ as the Mark−Houwink parameters,[30] a molecular weight of 2 700 000 g/mol is received for PS-2.5M, which is consistent with the value gained from SLS at 25 °C (2 400 000 g/mol).

The Staudinger index $[\eta]$ corresponds to the hydrodynamically effective volume of a particle divided by its mass. Since we are using the same PS sample for all measurements, changes in $[\eta]$ can directly be related to changes of the polymer volume. As a matter of fact, the Staudinger index decreases significantly with increasing SILS concentration c_{SILS}. In both solvent systems, a graphical representation of the results is given in Figure 3. Normalizing the Staudinger index at a variable SILS concentration by $[\eta]$ at $c_{\text{SILS}} = 0$ g/L allows for a better comparison of this structural change in both solvents (Figure 4).

If precipitation of PS chains at a phase boundary can be kinetically suppressed in solutions dilute enough, experiments may reveal a coil collapse. This collapse corresponds to an intramolecular phase separation while approaching the phase boundary. Thus, extrapo-

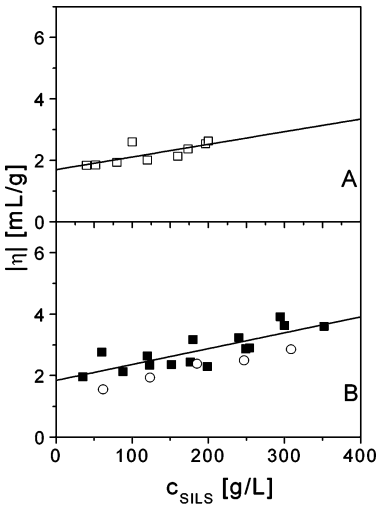

Figure 2. Reduced viscosities $|\eta|$ (eq 3) of SILS solutions in Tol−EthAc at 25 °C (A, □) and in toluene (B, 25 °C ■; 40 °C ○) are plotted against the SILS concentration c_{SILS}. The straight lines indicate eq 17 for measurements at 25 °C.

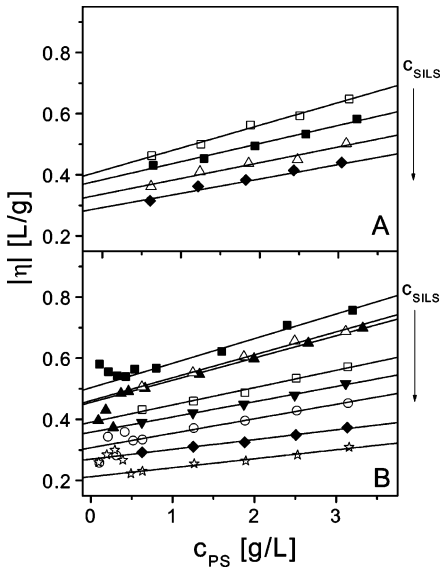

Figure 3. Reduced viscosities $|\eta|$ (eq 3) vs PS-2.5M concentration c_{PS} in Tol−EthAc (A) and in toluene (B) for different SILS concentrations at 25 °C. The straight lines are linear fits to data with $c_{\text{PS}} > 0.5$ g/L. The linear expressions are summarized in Table 2. The symbols denote in (A): □ ($c_{\text{SILS}} = 0$ g/L); ■ ($c_{\text{SILS}} = 69$ g/L); △ ($c_{\text{SILS}} = 147$ g/L); ♦ ($c_{\text{SILS}} = 192$ g/L). The symbols denote in (B): ■ ($c_{\text{SILS}} = 0$ g/L); △ ($c_{\text{SILS}} = 52$ g/L); ▲ ($c_{\text{SILS}} = 100$ g/L); □ ($c_{\text{SILS}} = 152$ g/L); ▼ ($c_{\text{SILS}} = 196$ g/L); ○ ($c_{\text{SILS}} = 249$ g/L); ◆ ($c_{\text{SILS}} = 305$ g/L); ☆ ($c_{\text{SILS}} = 352$ g/L).

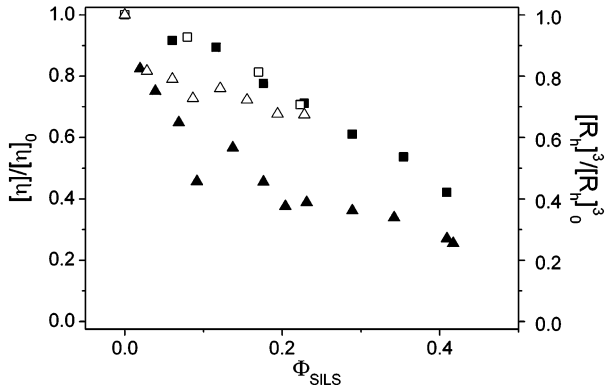

Figure 4. Staudinger index ($[\eta]$) and hydrodynamic volume ($[R_h]^3$) (DLS) of sample PS-2.5M are plotted against the volume fraction (eq 16) of SILS normalized by the corresponding value at $\Phi_{SILS} = 0$ ($[\eta]_0$; $[R_h]^3{}_0$). Open symbols represent measurements in Tol−EthAc (□ viscosimetry, △ DLS); closed symbols refer to measurements in toluene (■ viscosimetry, ▲ DLS). Measurements are performed at 25 °C.

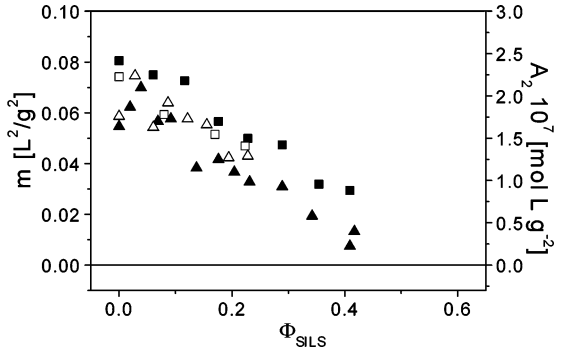

Figure 5. Measure of solvent quality for PS chains expressed by the slope m of eq 4 from viscosimetry (toluene ■; Tol−EthAc □) and by A_2 values gained from SLS (toluene ▲; Tol−EthAc △). The zero level indicates θ-conditions.

lation of Φ_{SILS} to $[\eta] = 0$ may indicate the limit of a coil collapse and the onset of phase instability. As is shown in Figure 4, such a limit is expected at $\Phi_{SILS} \sim 0.55$ in both solvent systems. Additionally, Figure 4 represents the normalized hydrodynamically effective volume of PS-2.5M calculated with R_h from DLS measurements. Although the points do not overlay, both methods show the same trend.

Further information on solvent quality can be extracted from the slope m in eq 4. If no increase of the reduced viscosity with c_{PS} is observed, the solvent can be referred to as a θ-solvent. Similar tendencies can be expected for A_2 values taken from SLS. Figure 5 shows both the slope m of eq 4 and A_2 values as a function of c_{SILS}. In fact, both parameters decrease and approach zero, with increasing c_{SILS}. The decreasing solvent quality for PS with increasing SILS concentration is in good agreement with the observed shrinking of PS dimensions in solution. Even more, the expected volume fraction, where A_2 and m approach zero, is in the same region as indicated by the shrinking dimensions of the PS chain based on $[\eta]$.

Three different PS samples with molecular weights of 270 000, 870 000, and 2 400 000 g/mol are investigated in SILS solutions as solvents by light scattering experiments. Characteristic parameters of all three samples are summarized in Table 3. Light scattering experiments on pure SILS solutions are necessary since they serve as solvents for the PS chains and therefore have to be subtracted from the scattering intensity of

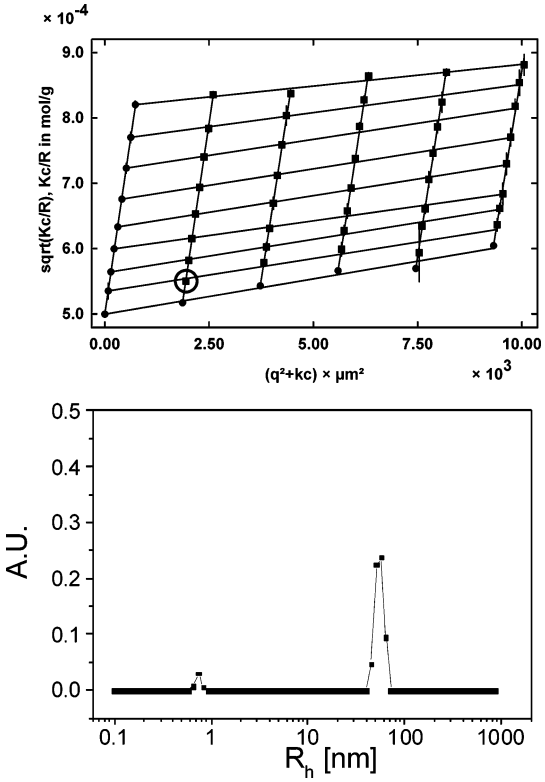

Figure 6. Simultaneous recording of SLS and DLS shown for a measurement of a solution of PS-2.5M in toluene with $c_{SILS} = 152$ g/L at 25 °C. Top: The square root of the scattering ratio is plotted as indicated in eq 9. The circle marks the corresponding angle, where the DLS measurement shown below is performed. Bottom: A typical result of a CONTIN analysis from a DLS measurement at $\theta = 30°$.

PS solutions. Because of their small size and hollow structure, which corresponds to a low molecular weight, even in toluene as the solvent an excess scattering of only 5% at $c_{SILS} = 360$ g/L is observed. Figure 6 gives a typical result of a combined SLS and DLS measurement of sample PS-2.5M. Data are received at a SILS concentration of 152 g/L in toluene as the solvent. The CONTIN analysis clearly resolves two relaxation times: one stemming from the SILS molecules with a radius of about 0.7 nm and the other stemming from the PS chains.

As is shown in Figures 7A and 8A, the chain dimensions of the sample PS-2.5M given by R_g and R_h shrink with increasing SILS concentration c_{SILS}. This observation is made in both solvent systems. Additional information is expected from a discussion of molar mass data in the two solvents.

The case of Tol−EthAc represents the isorefractive case for SILS. The values are calculated using the refractive index increment of PS in Tol−EthAc determined without any SILS. In line with the isorefractivity of SILS and Tol−EthAc, the molecular weight of the PS chains determined by SLS keeps constant over the whole c_{SILS} regime in this solvent mixture. Although only shown explicitly for PS-2.5M in Figure 7B, this behavior is found for all three samples investigated. Unfortunately, the solubility of SILS in this solvent mixture is lower than in pure toluene. As a consequence, the extent of coil shrinking does not become as strong as observed in the case of toluene as the solvent.

A completely different trend of the molecular mass values is revealed in toluene (Figure 8B). If the refrac-

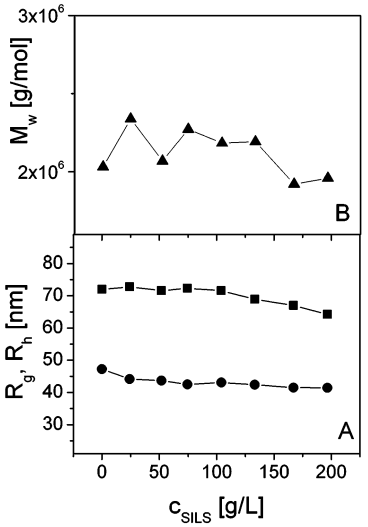

Figure 7. Light scattering results for PS-2.5M in Tol−EthAc at different SILS concentrations c_{SILS}. Measurements are performed at 25 °C. Molecular weight M_w (▲); radius of gyration R_g (■); hydrodynamically effective radius R_h (●).

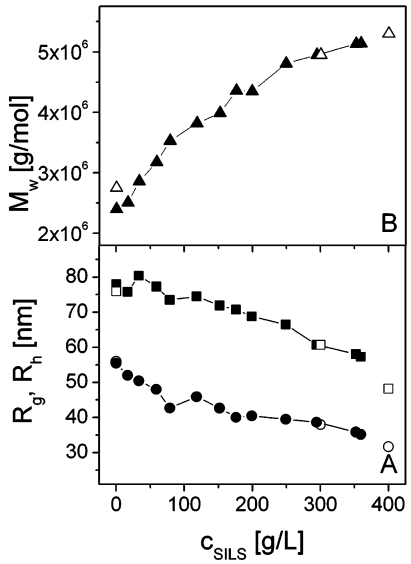

Figure 8. Light scattering results for PS-2.5M in toluene at different SILS concentrations c_{SILS}. Molecular weight M_w (▲, △); radius of gyration R_g (■, □); hydrodynamically effective radius R_h (●, ○). Closed symbols refer to measurements at 25 °C and open symbols to measurements at 40 °C.

tive index increment of PS in pure toluene is used to calculate M_w, its molecular weight values increase with c_{SILS} up to twice the value measured at $c_{SILS} = 0$. Again this trend could be reproduced with two other PS samples PS-250K and PS-950K in toluene at 25 °C, not shown in the Figure. SILS and toluene are not isorefractive, and addition of SILS to toluene thus modifies the scattering contrast of PS in solution.

An explanation for the increase of the apparent molar mass of the PS chains may be the exclusion of SILS molecules from the center of the polymer coils. This inability to completely penetrate the PS coils leaves solvent domains depleted from SILS molecules with the lowest SILS concentration in the interior of the coils. The depletion domains correspond to a preferential desorption of the colloidal SILS particles as one of the two solvent components.

The scattering of this depleted zones is superimposed to the scattering of the PS coils. If the sign of the

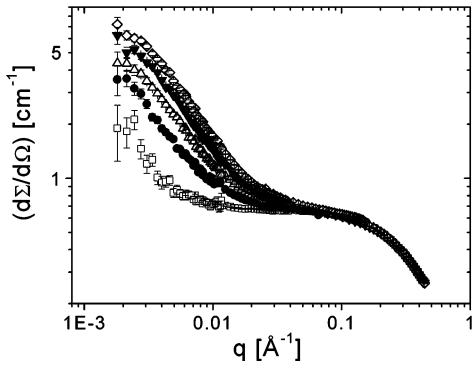

Figure 9. SANS curves of D8-PS in D8-toluene in the presence of 320 g/L SILS. The symbols refer to the following PS concentrations (in g/L): 0 (□), 0.625 (●), 1.250 (△), 1.875 (▼), and 2.500 (◇).

(dn/dc) value of SILS in toluene $(dn/dc)_{SILS}$ is opposite to the sign of $(dn/dc)_{PS}$ of PS in toluene, the net scattering of the [PS + depleted zone] is larger than the corresponding scattering of PS in pure toluene. As a consequence, the resulting apparent mass values are larger than the real molar mass of the corresponding polymer chains. In fact, the $(dn/dc)_{SILS}$ in toluene was determined to $(dn/dc)_{SILS} = -0.073$ mL/g, supporting our interpretation of the excess molar mass values. Proper values for the molar mass of PS chains in toluene−SILS mixtures could be established if $(dn/dc)_{PS}$ would be determined at constant chemical potentials of SILS at the respective SILS concentration.[31] However, determination of $(dn/dc)_{PS}$ at various SILS concentrations under constant chemical potential of SILS is rather cumbersome. In light of the low significance of an additional mass determination in toluene + SILS, carrying out these tedious experiments was not considered to be justified.

Further indications for the polymer-induced depletion of SILS could be provided by two supplementary experiments: SANS and the record of the crystallization behavior of SILS in a PS−toluene solution. Results from both experiments shall be outlined in the following.

SANS offered an exceptional opportunity to perform experiments with a scattering contrast which perfectly complements SLS. By applying fully deuterated polystyrene (D8-PS) and D8-toluene, the only contrast giving rise to an angular dependent excess scattering is the one stemming from SILS embedded in an isotropically scattering, deuterated matrix. It was our hope to generate a ternary solution, which permits to investigate the impact of an "invisible" polymer chain on the distribution of the SILS molecules. Figure 9 shows the scattering cross section of SILS at four different D8-PS concentrations. Two angular dependent regimes become discernible. A decrease at low q depends on the polymer concentration and reflects a structural feature of the polymer chains becoming transparent through the contrast of SILS. All five curves converge to an intermediate plateau at $q = 0.07$ Å^{-1} which precedes a second drop. The second drop does not depend on the polymer concentration and therefore can be attributed to SILS. In fact, a Guinier analysis of the scattering curves in a regime of 0.033 Å$^{-1} < q < 0.15$ Å^{-1} leads to a radius of gyration of $R_g = 0.6$ nm, in perfect agreement with the size of a single SILS molecule (0.705 nm, ref 20).

The low-q regime is analyzed by means of a conventional Zimm analysis. The scattering data under consideration are derived from the original scattering cross

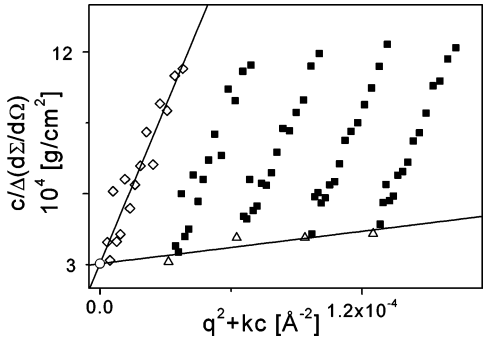

Figure 10. Net intensities of D8-PS (■) calculated according to eq 14 in D8-toluene using a solution of 320 g/L SILS as the solvent in SANS experiments. Linear extrapolation toward zero concentration c (◇) and zero scattering vector q (△) are shown.

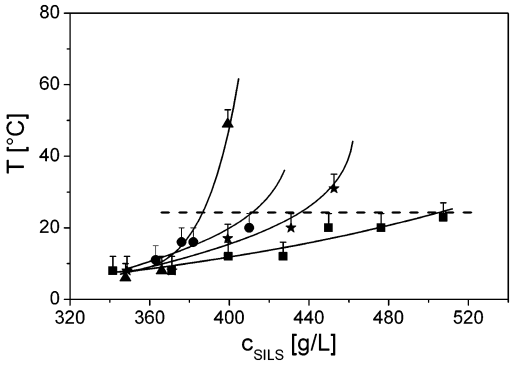

Figure 11. Crystallization diagram of SILS−PS solutions in toluene. The lines are given to guide the eye. Above and left of these lines a one-phase regime occurs. The symbols refer to the following PS concentrations (in g/L): 0 (■), 0.432 (★), 0.48 (●), and 0.648 g/L (▲). The dashed line shows an isotherm at 25 °C. The intersections with the four curves are shown as closed triangles in Figure 12A.

section shown in Figure 9 by subtracting the sample background (eq 14). Sample background is a polymer-free SILS solution in D8-toluene at the same SILS concentration $c_{SILS} = 320$ g/L as applied for the four polymer solutions of D8-PS. The resulting Zimm diagram is shown in Figure 10. Evaluation of the angular dependence leads to a radius of gyration of $R_g = 47 \pm 3$ nm. This radius of gyration measures the spatial scattering contrast distribution stemming from the depletion zone. The depletion zone certainly does not adopt a regular sphere with a sharp boundary but corresponds to a domain having the same center of mass as the depleting PS chain and with the SILS concentration decreasing with decreasing distance from this center of mass. The radius of gyration of this zone measured by SANS has to be compared with the radius of gyration of the D8-PS coils. Unfortunately, a radius of gyration for those PS chains cannot be given explicitly. We can only estimate an upper limit of R_g of the PS chains in the respective solvent system by means of $R_h = 26$ nm from DLS via ρ. Even under the assumption of $\rho = 1.53$—which corresponds to an upper limit as the actual chains are considered to be more compact than Gaussian coils—the estimated radius of gyration of the PS chains is $R_g = 1.53 \times 26$ nm $= 40$ nm. This upper limit is already lower than the R_g of the depletion zone, suggesting that the depletion zone is significantly larger than the monomer cloud of the PS chains.

Another strong hint indicating a SILS depleted solvent zone is obtained by investigating crystallization of SILS in PS−SILS−toluene mixtures. As is shown in Figure 11, the threshold concentration c_{SILS} where SILS crystals first appear is significantly decreased by adding PS chains to the solution. The decrease becomes more pronounced the larger the PS concentration gets. This behavior can be explained by the exclusion of SILS molecules from the domain of the polymer coil, leading to an increase of the SILS concentration outside the polymer chains. Thus, the crystallization threshold is reached at lower SILS concentrations compared to PS-free solutions. We consider this behavior also to represent first principles of the mode of action of polymeric crystallization aids used for example in the field of protein crystallization. We have to emphasize, though, that these principles can at best reflect part of the reality. For example, water-soluble proteins generally bear electrical charges to mention just one additional aspect not considered by these principles.

As a consequence, we could provide some indication for the depletion of the polymer domains from SILS molecules. This depletion raises the concentration of SILS around the polymer chains, leading to a decrease of the SILS entropy. The SILS molecules try to relax by exerting a pressure on the chain dimensions. However, depletion of the SILS molecules from the polymer domains may not be the only cause of chain shrinking. If the small spheres approach the size of a solvent molecule, the insolubility of PS in sphere solutions becomes indistinguishable from a simple solvent quality effect, comparable for instance to adding ethanol as a nonsolvent for PS to a PS solution in toluene.

To gain additional information, we evaluated the phase behavior of CP mixtures in solution over a wide range of PS and SILS concentrations. Results can readily be discussed in terms of phase diagrams with a plot of polymer concentration vs colloid content constituting the liquid−liquid coexistence curve. Theoretical calculations of the phase behavior in the protein limit predict a considerable narrowing of the one phase regime if the solvent quality for the polymer chains decreases from good solvent conditions to θ-conditions.[7,8] In the case of good solvents and $R_g/R_c > 3$, Bolhuis et al.[8] by means of computer simulations found a dramatic increase of the coexistence curve as soon as the colloid volume fraction dropped below 0.4. Under θ-conditions and $R_g/R_c > 3$, a one-phase regime only appeared below a colloid volume fraction of 0.1 where the coexistence curve again exhibits a steep ascent toward lower colloid volume fractions. For a comparison with the present results, we have to keep in mind that the one-phase regime shrinks considerably with increasing R_g/R_c.

In fact, for $c_{PS} \leq 25$ g/L in the good solvent system PS−SILS−toluene, a two-phase regime did not show until c_{SILS} exceeds 350 g/L. Above this limit, a coexistence curve with a steep descent turns into an almost horizontal line at very low c_{PS} values, which separates a one-phase regime from a two-phase regime with insoluble SILS crystals. This phase behavior can be easily related to the crystallization diagram of Figure 11, where the quasi-horizontal section of the coexistence curve is recovered as the 25 °C isotherm, crossing the four curves corresponding to constant values of c_{PS}. Also in line with the predictions of Bolhuis et al.,[8] only a very small one-phase regime appeared in the case of PS−SILS−cyclohexane at 35 °C. In the latter case, which is a θ-system for PS, the coexistence curve did only become noticeable once the colloid volume fraction

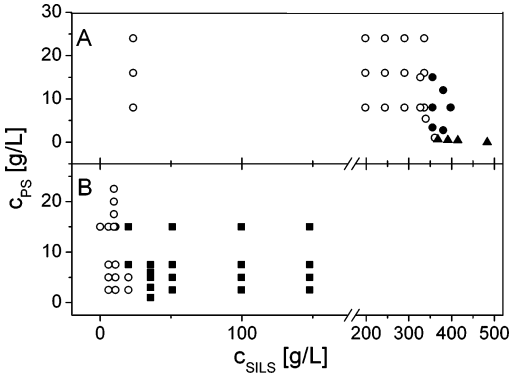

Figure 12. Phase diagram of the system PS-2.5M−SILS as PS concentration vs SILS concentration in toluene at 25 °C (A) and in cyclohexane at 35 °C (B). In toluene, the PS chains are considered to be fully interacting whereas in cyclohexane, the PS chains are noninteracting. Open symbols represent a single phase and closed symbols two phases. Closed triangles (▲) correspond to intersections of the isotherm at 25 °C with the four curves shown in Figure 11.

dropped below 0.05. Results are summarized in Figure 12.

Summary

Hydrodynamic and geometric dimensions of PS coils in good solvents are investigated as a function of SILS concentration within a regime of 0 g/L < c_{SILS} < 350 g/L. Coil dimensions significantly decrease with increasing SILS concentration. This shrinking is at least in part induced by a depletion effect from the SILS molecules. It can be verified by various experiments, leading to the following results: The molecular weight values obtained in isorefractive and nonisorefractive solvents for SILS differ significantly. Whereas molar mass data of PS remain unaffected in the isorefractive solvent, corresponding values increase with increasing c_{SILS} in the nonisorefractive solvent due to an additional scattering contribution from the depletion zone. SANS measurements also indicate a domain depleted from SILS. The domain is larger than the radius of gyration of the displacing PS coils. Solutions with PS lead to a decreased solubility of SILS. This decrease is more pronounced the more PS is added. The effect is considered to bear some analogy to the use of water-soluble polymers as crystallization aids for proteins. The phase behavior of PS−SILS in solvents considered to be good solvents for PS are strikingly different from the respective behavior for PS−SILS with PS under θ-conditions. In agreement with theoretical predictions for the protein limit of CP mixtures, a declining solvent quality for PS leads to a considerable narrowing of the one-phase regime of CP solutions. We consider these results as a strong indication for PS/SILS mixtures to be an appropriate model system for CP mixtures in the protein limit because the mass and volume of SILS particles are still an order of magnitude larger than the respective parameters of a conventional solvent molecule. However, we have to state that differentiation between the protein limit and a mixture of two small molecular solvents becomes obsolete, once the particles of both solvent components get equal in size.

Acknowledgment. We gratefully acknowledge the synthetic work performed by Christoph Kress. Dr. Paul van der Schoot is thanked for helpful discussions. This work is supported by the Deutsche Forschungsgemeinschaft, Project HU 807/5-1.

References and Notes

(1) Asakura, S.; Oosawa, F. *J. Chem. Phys.* **1954**, *22*, 1255. Asakura, S.; Oosawa, F. *J. Polym. Sci.* **1958**, *33*, 183.
(2) Poon, W. C. K. *J. Phys.: Condens. Matter* **2002**, *14*, R859.
(3) Tuinier, R.; Rieger, J.; de Kruif, C. G. *Adv. Colloid Interface Sci.* **2003**, *103*, 1.
(4) de Gennes, P. G. *C. R. Acad. Sci. B* **1979**, *288*, 359.
(5) Tuinier, R.; Dhont, J. K. G.; de Kruif, C. G. *Langmuir* **2000**, *16*, 1497.
(6) Sear, R. P. *Phys. Rev. Lett.* **2001**, *86*, 4696.
(7) Sear, R. P. *Phys. Rev. E* **2002**, *66*, 051401.
(8) Bolhuis, P. G.; Meijer, E. J.; Louis, A. A. *Phys. Rev. Lett.* **2003**, *90*, 068304.
(9) Sear, R. P. *Phys. Rev. E* **1998**, *58*, 724.
(10) van der Schoot, P. *Macromolecules* **1998**, *31*, 4635.
(11) Kramer, T.; Maskos, M.; Scholz, S.; Huber, K. *J. Colloid Interface Sci.* **2004**, *279*, 447.
(12) Markovic, I.; Ottewill, R. H.; Cebula, D. J.; Field, I.; Marsh, J. F. *Colloid Polym. Sci.* **1984**, *262*, 648.
(13) Husein, M.; Rodil, E.; Vera, J. *Langmuir* **2003**, *198*, 467.
(14) Antonietti, M.; Bremser, W.; Müschenborn, D.; Rosenauer, C.; Schupp, B. *Macromolecules* **1991**, *24*, 6636.
(15) Jungmann, N.; Schmidt, M.; Maskos, M. *Macromolecules* **2001**, *34*, 8347.
(16) Jungmann, N.; Schmidt, M.; Maskos, M. *Macromolecules* **2002**, *35,* 6851.
(17) Baumann, F.; Deubzer, B.; Geck, M.; Dauth, J.; Schmidt, M. *Macromolecules* **1997**, *30*, 3568.
(18) Lindenblatt, G.; Schärtl, W.; Pakula, T.; Schmidt, M. *Macromolecules* **2000**, *33*, 9340.
(19) Dittmar, U.; Hendan, B. J.; Flörke, U.; Marsmann, H. C. *J. Organomet. Chem.* **1995**, *489*, 185.
(20) Azinovic, D.; Cai, J.; Eggs, C.; König, H.; Marsmann, H. C.; Veprek, S. *J. Lumin.* **2002**, *97*, 40.
(21) Dittmar, U. Ph.D. Thesis, University of Paderborn, 1993.
(22) *Manuel Jakubith, Grundoperationen und chemische Reaktionstechnik*; Wiley-VCH: Weinheim, 1998.
(23) (a) Zimm, B. H. *J. Chem. Phys.* **1948**, *16*, 1093. (b) Berry, G. C. *J. Chem. Phys.* **1966**, *44*, 4550.
(24) Koppel, D. E. *J. Chem. Phys.* **1972**, *57*, 4818.
(25) Provencher, S. W. *Comput. Phys.* **1982**, *272*, 13, 229.
(26) Lindner, P. *J. Appl. Crystallogr.* **2000**, *33*, 807.
(27) Lindner, P. In *Neutrons, X-rays and Light: Scattering Methods Applied to Soft Condensed Matter;* Lindner, P.; Zemb, Th., Eds.; Elsevier: Amsterdam, 2002; p 23.
(28) Einstein, A. *Ann. Phys.* **1911**, *33*, 591.
(29) Knappe, W.; Lange, H. *Kolloid-Z.* **1961**, *179/2*, 97.
(30) Brandrup, J. *Polymer Handbook*, 3rd ed.; John Wiley: New York, 1996.
(31) Stockmayer, W. H. *J. Chem. Phys.* **1950**, *18*, 58.
(32) Landolt-Börnstein, Springer: Berlin, Vol. III/38A.
(33) *CRC Handbook of Chemistry and Physics*; CRC Press: Boca Raton, FL, 1993.

MA048766X